

CrossMark  
click for updatesCite this: *Catal. Sci. Technol.*, 2015,  
5, 5048

## Recent progress in g-C<sub>3</sub>N<sub>4</sub> based low cost photocatalytic system: activity enhancement and emerging applications

Shengming Yin,<sup>a</sup> Jianyu Han,<sup>ab</sup> Tianhua Zhou<sup>ac</sup> and Rong Xu<sup>\*a</sup>

Graphitic C<sub>3</sub>N<sub>4</sub> (g-C<sub>3</sub>N<sub>4</sub>) has continuously attracted attention since it was reported as a metal-free semiconductor for water splitting. However, its ability to evolve hydrogen from water is significantly dependent on the use of noble metal co-catalyst, mainly Pt. In recent years, good progress has been achieved in developing co-catalysts containing earth abundant elements only for constructing low cost and efficient g-C<sub>3</sub>N<sub>4</sub> based photocatalytic systems. Besides, exfoliation of bulk g-C<sub>3</sub>N<sub>4</sub> into two dimensional g-C<sub>3</sub>N<sub>4</sub> nanosheets offers large surface area and exposed active sites, which are beneficial for activity enhancement. Furthermore, oxygen evolution and CO<sub>2</sub> photoreduction over g-C<sub>3</sub>N<sub>4</sub> have gained increasing interests due to the demand to achieve overall water splitting and conversion of CO<sub>2</sub> into chemicals and fuels. In this mini-review, we will briefly summarize the latest research works on g-C<sub>3</sub>N<sub>4</sub> based photocatalytic systems during the last three years with emphasis on the progress achieved in enhancing the hydrogen evolution activity of g-C<sub>3</sub>N<sub>4</sub> by loading noble metal free co-catalysts, exfoliating bulk g-C<sub>3</sub>N<sub>4</sub> into nanosheets, and applying the g-C<sub>3</sub>N<sub>4</sub> system in photocatalytic O<sub>2</sub> evolution and CO<sub>2</sub> reduction.

Received 23rd June 2015,  
Accepted 14th July 2015

DOI: 10.1039/c5cy00938c

www.rsc.org/catalysis

### 1. Introduction

Energy and environmental problems have become more and more severe over the recent years due to the overuse of fossil fuels and uncontrolled CO<sub>2</sub> emission from the combustion of

fossil fuels. It is of utmost urgency to find green technology to address these concerns.<sup>1</sup> One promising method is the utilization of solar energy with the help of semiconductor photocatalysts. A process known as photocatalytic water splitting converts water into H<sub>2</sub> which is considered to be a promising clean energy source to replace fossil fuels;<sup>2</sup> another process called artificial photosynthesis is focused on synthesizing hydrocarbon molecules from CO<sub>2</sub> which is a mimic of the natural photosynthesis in green plants.<sup>3</sup>

Since Fujishima reported a photoelectrochemical (PEC) water splitting process by using a TiO<sub>2</sub> photoanode, researchers have spent efforts on improving the conversion

<sup>a</sup> School of Chemical & Biomedical Engineering, Nanyang Technological University, 62 Nanyang Drive, Singapore 637459. E-mail: rxu@ntu.edu.sg; Fax: +65 67947553; Tel: +65 67906713

<sup>b</sup> Energy Research Institute @ NTU, Nanyang Technological University, 50 Nanyang Drive, Singapore 637553

<sup>c</sup> SinBeRISE CREATE, National Research Foundation, CREATE Tower Level 11, 1 Create way, Singapore 138602



Shengming Yin

Shengming Yin received his bachelor and master's degree in Materials Science and Engineering at Huazhong University of Science and Technology, China in 2010 and 2013. He is now pursuing his PhD degree under the supervision of Prof. Xu at Nanyang Technological University. His research interest focuses on the design of noble-metal free photocatalytic systems for water splitting.



Jianyu Han

Jianyu Han received his bachelor's degree in Chemistry from Nanjing University, China in 2011. As a graduate student in Nanyang Technological University, he concentrates on solar fuel production from photocatalytic water splitting and photocatalytic carbon dioxide reduction.



efficiency of this process.<sup>4</sup> Various semiconductors, *e.g.* oxide, (oxy)nitride, and (oxy)sulfide, have been shown capable of splitting water under light irradiation with suitable co-catalysts deposited on the surface.<sup>5–7</sup> Unfortunately, the relatively low efficiency and noble metal-containing materials of these systems make them unfavourable for practical usage. The price of H<sub>2</sub> by this method is still much higher than expected. Further improving the solar to hydrogen (STH) efficiency and reducing the cost are of particular significance to realize the potential of this technology. Compared to water splitting, the study of CO<sub>2</sub> photoreduction is still in its infancy partially due to the fact that it is energetically more difficult to reduce CO<sub>2</sub> than proton. CO<sub>2</sub> reduction requires a much larger driving force than water reduction (Table 1).<sup>8</sup> In addition, CO<sub>2</sub> reduction is a multiple electron process, which makes it kinetically harder to proceed. The selectivity to products is also an important aspect in CO<sub>2</sub> reduction. After all, the development of photocatalytic water splitting and CO<sub>2</sub> reduction depends on the efficient utilization of solar power and the enhancement of catalytic conversion of water and CO<sub>2</sub> into fuels and chemicals. These serve as the criteria for the selection of suitable photocatalysts.

Graphitic carbon nitride (g-C<sub>3</sub>N<sub>4</sub>), also known as “melon”, is the most stable allotrope among different carbon nitride materials. It can be synthesized *via* thermal condensation of low cost nitrogen-rich precursors such as cyanamide, dicyandiamide, melamine, thiourea and urea. It has a graphene-like structure consisting of two-dimensional frameworks of tri-s-triazine connected *via* tertiary amines. This unique structure and high degree of condensation make g-C<sub>3</sub>N<sub>4</sub> stable at elevated temperatures as high as 600 °C and in different chemical environments (acid, base or organic solvent). Furthermore, this tri-s-triazine ring structure makes it an indirect semiconductor with a band gap of ~2.7 eV, corresponding to an optical wavelength of 460 nm in the visible light range.<sup>9,10</sup> In 2009, Wang *et al.* reported that photocatalytic water splitting can be achieved using this metal-free

**Table 1** CO<sub>2</sub> reduction potentials (reported at pH 7). Adapted with permission from ref. 8. Copyright 2009 American Chemical Society

Reaction	E° (V) vs. SCE
CO <sub>2</sub> + 2H <sup>+</sup> + 2e <sup>-</sup> → HCO <sub>2</sub> H	-0.85
CO <sub>2</sub> + 2H <sup>+</sup> + 2e <sup>-</sup> → CO + H <sub>2</sub> O	-0.77
CO <sub>2</sub> + 4H <sup>+</sup> + 4e <sup>-</sup> → C + 2H <sub>2</sub> O	-0.44
CO <sub>2</sub> + 4H <sup>+</sup> + 4e <sup>-</sup> → HCHO + H <sub>2</sub> O	-0.72
CO <sub>2</sub> + 6H <sup>+</sup> + 6e <sup>-</sup> → CH <sub>3</sub> OH + H <sub>2</sub> O	-0.62
CO <sub>2</sub> + 8H <sup>+</sup> + 8e <sup>-</sup> → CH <sub>4</sub> + 2H <sub>2</sub> O	-0.48

polymeric g-C<sub>3</sub>N<sub>4</sub>.<sup>11</sup> Since then, enormous attention has been drawn to g-C<sub>3</sub>N<sub>4</sub> because it is ideal for the construction of low cost photocatalysts. Nevertheless, the photoactivity of g-C<sub>3</sub>N<sub>4</sub> suffers from several main drawbacks. Firstly, the relatively large band gap (2.7 eV) limits its effective utilization of visible light of longer wavelengths. It was estimated that a photocatalyst with a band gap as narrow as 1.8–2.0 eV and suitable band positions would be desirable from the viewpoint of both solar energy harvesting and surface kinetics of water splitting reactions.<sup>12</sup> Secondly, the low charge carrier mobility inhibits the separation and transportation of electrons and holes. It was revealed by both first principle calculations and experimental results that the charge carrier mobility of the pristine g-C<sub>3</sub>N<sub>4</sub> can be enhanced by doping non-metal elements which widen the valence band (VB) of g-C<sub>3</sub>N<sub>4</sub>.<sup>13–16</sup> Furthermore, the surface inertness of g-C<sub>3</sub>N<sub>4</sub> due to the nature of the covalent bond leads to the low reaction rates of hydrogen and oxygen evolution half reactions.<sup>9</sup> The surface area of bulk g-C<sub>3</sub>N<sub>4</sub> is generally small since it is prepared by condensation of organic precursor compounds at high temperature. There also exist rich grain boundary defects on the surface of g-C<sub>3</sub>N<sub>4</sub> resulting from incomplete condensation, which may cause the recombination of excited charges.<sup>17</sup>

As a result, the efforts that have been made to address these issues include modification of the electronic structure



Tianhua Zhou

*Dr. Tianhua Zhou received his PhD at Fuzhou University, China in 2008 under the supervision of Prof. Jian-Xi Zhao. Then he joined Prof. Jiang-Gao Mao's group as a research assistant professor. Since 2012, he has been a research fellow in Prof. Rong Xu's group at Nanyang Technological University. His current research interests focus on the development of new photo-(electro) catalysts for water oxidation, hydrogen evolution, and carbon dioxide conversion.*

*tion, and carbon dioxide conversion.*



Rong Xu

*Prof. Rong Xu received her PhD degree in Chemical Engineering (2004) from the National University of Singapore. She joined the School of Chemical & Biomedical Engineering at Nanyang Technological University in 2004 and she is currently an Associate Professor there. Her main research interests include the development of semiconductors and molecular photocatalysts for solar energy conversion, and fabrication of nanostructured materials for biomedical and environmental applications.*

*rials for biomedical and environmental applications.*



of  $g\text{-C}_3\text{N}_4$  by integrating certain organic molecules into its ring structure,<sup>18,19</sup> doping metal or non-metal ions in the bulk structure of  $g\text{-C}_3\text{N}_4$  to form an impurity level in its forbidden band to improve its visible light absorption properties,<sup>14,15,20–23</sup> and suppression of electron–hole recombination by forming composites of  $g\text{-C}_3\text{N}_4$  and other semiconductors with suitable band alignment or carbon materials to improve the charge transportation.<sup>24–28</sup> Sensitization of the pristine  $g\text{-C}_3\text{N}_4$  by organic dyes or quantum dots is also efficient to enhance its performance under visible light.<sup>29,30</sup> Besides, morphology control of  $g\text{-C}_3\text{N}_4$  to increase the specific surface area as well as to expose the active sites for photocatalytic reaction is another strategy to achieve photocatalytic activity improvement. Mesoporous  $g\text{-C}_3\text{N}_4$  (mpg- $\text{C}_3\text{N}_4$ ) is commonly prepared using  $\text{SiO}_2$  nanospheres as the template.<sup>31</sup> In addition,  $g\text{-C}_3\text{N}_4$  with other morphologies such as spherical nanoparticles,<sup>32</sup> nanorods,<sup>33–35</sup> hollow spheres,<sup>36,37</sup> and ordered 3D structures<sup>38</sup> have been prepared using template or non-template methods. There are many literature reports demonstrating the use of such modifications to improve the performance of the  $g\text{-C}_3\text{N}_4$  system, which has been shown as a promising material for solar fuel production.

In this mini review, we intend to summarize the recent progress in the development of efficient and low cost  $g\text{-C}_3\text{N}_4$  systems on a few important aspects including deposition of noble metal free cocatalysts on  $g\text{-C}_3\text{N}_4$ , exfoliation of bulk  $g\text{-C}_3\text{N}_4$  into  $g\text{-C}_3\text{N}_4$  nanosheets and application of  $g\text{-C}_3\text{N}_4$  in water oxidation, overall water splitting and  $\text{CO}_2$  photoreduction. These challenging research areas have drawn increasing interests from many research groups including our own. Some review articles have been recently published focusing on the fabrication, chemical modification, bandgap engineering and heterostructure formation of  $g\text{-C}_3\text{N}_4$  based photocatalysts.<sup>9,10,17,28,39</sup> We believe that this review would be a good complement to the literature on  $g\text{-C}_3\text{N}_4$  based photocatalyst systems.

## 2. Noble metal free $g\text{-C}_3\text{N}_4$ system

Depositing a suitable cocatalyst on the surface of a semiconductor is of great importance to improve its efficiency. Cocatalysts significantly enhance the surface reaction rate by lowering the activation energy and facilitate the separation of electrons and holes by forming a Schottky junction between the semiconductor and the cocatalyst. The role of the cocatalyst in photocatalysis and photoelectrocatalysis has been well reviewed by Yang *et al.*<sup>40</sup>

Pt is so far the most efficient and commonly used cocatalyst of  $g\text{-C}_3\text{N}_4$  for hydrogen production. Despite that, a series of non-noble metal containing hydrogen evolution reaction (HER) electrocatalysts have been explored; however, only a few of them are successfully deposited on  $g\text{-C}_3\text{N}_4$  as cocatalysts.<sup>41</sup> To further reduce the cost of  $g\text{-C}_3\text{N}_4$  based photocatalysts and make them available for

industrial usage, noble metal free cocatalysts are highly needed.

As a pioneering work in this area, Dong *et al.* reported in 2012 that a molecular cocatalyst  $\text{Ni}(\text{TEOA})_2\text{Cl}_2$  can be used in the system of  $g\text{-C}_3\text{N}_4$  to replace Pt for stable hydrogen evolution.<sup>42</sup> In this system,  $g\text{-C}_3\text{N}_4$  plays the main role of light absorber.  $\text{Ni}(\text{TEOA})_2\text{Cl}_2$  is formed *via* self-assembly of  $\text{Ni}^{2+}$  ions and triethanolamine (TEOA) which is the sacrificial reagent in solution. A similar nickel-containing complex, nickel–thiourea–triethylamine ( $\text{Ni-TU-TETN}$ ), formed *in situ* during photocatalytic reaction, was also reported to be an active cocatalyst on the surface of  $g\text{-C}_3\text{N}_4$  for hydrogen production.<sup>43</sup> But the quantum efficiency (QE) obtained using  $\text{Ni-TU-TETN}/g\text{-C}_3\text{N}_4$  is only 0.2% at 400 nm irradiation, which is much smaller than 1.51% at 400 nm reported for  $\text{Ni-TEOA}/g\text{-C}_3\text{N}_4$ .  $\text{Co}(\text{dmgH})_2\text{pyCl}$  has been studied as an electrocatalytic HER catalyst and was used for photocatalytic hydrogen production in a homogeneous system as well.<sup>44</sup> When coupled with  $g\text{-C}_3\text{N}_4$  in TEOA solution, it was able to produce hydrogen under visible light. The highest QE of this system was 0.62% under 365 nm irradiation.<sup>45</sup> However, the activity decreased dramatically after 8 h of photocatalytic reaction due to the decomposition of  $\text{Co}(\text{dmgH})_2\text{pyCl}$ . To overcome this, a more stable  $\text{Ni}(\text{dmgH})_2$  HER catalyst was used to construct a  $\text{Ni}(\text{dmgH})_2/g\text{-C}_3\text{N}_4$  photocatalyst.  $\text{Ni}(\text{dmgH})_2$  sub-microcrystals were grown on  $g\text{-C}_3\text{N}_4$  *via* a simple precipitation method. Its activity remained almost the same after three recycle runs, indicating the enhanced stability of this system although the activity needs to be further improved.<sup>46</sup>

Besides the transition metal containing complexes, some inorganic compounds have also been coupled with  $g\text{-C}_3\text{N}_4$  for the construction of noble metal free  $g\text{-C}_3\text{N}_4$  photocatalysts. For example, our group has successfully deposited NiS on  $g\text{-C}_3\text{N}_4$  *via* a facile hydrothermal method.<sup>47</sup> An aqueous solution of nickel acetate (NiAc) and thioacetamide was used for the synthesis of NiS in the presence of mpg- $\text{C}_3\text{N}_4$ , allowing  $\text{Ni}^{2+}$  and the sulfur precursor to enter into the pores of mpg- $\text{C}_3\text{N}_4$  for the formation of a nanosized and well-disperse NiS

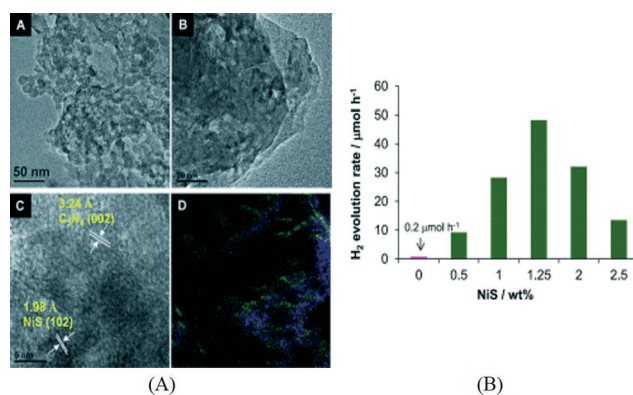


Fig. 1 (A) TEM, HRTEM and element mapping images of NiS/mpg- $\text{C}_3\text{N}_4$ ; (B) effect of NiS cocatalyst loading on hydrogen production.<sup>47</sup> Copyright 2013 WILEY-VCH Verlag GmbH & Co. KGaA Weinheim.



cocatalyst. The formation of NiS nanoparticles was confirmed by high resolution transmission electron microscopy (HRTEM) analysis, element mapping and X-ray photoelectron spectroscopy (XPS). The typical HRTEM images and elemental mapping results are shown in Fig. 1A. The loading of NiS has a significant effect on the activity and the optimum NiS loading was found to be 1.25 wt% (Fig. 1B). For comparison, the activity of a mixture of mpg-C<sub>3</sub>N<sub>4</sub> and pre-synthesized NiS was much lower than that of NiS/mpg-C<sub>3</sub>N<sub>4</sub>, which is due to the poor interface between NiS and mpg-C<sub>3</sub>N<sub>4</sub> and the relatively larger particle size of pre-synthesized NiS. A high QE of 1.9% at 440 nm was obtained over the optimized NiS/mpg-C<sub>3</sub>N<sub>4</sub> photocatalyst. The same photocatalyst demonstrates good stability with 84% of the initial activity retained after 4 runs of photoreaction. Subsequently, Chen *et al.* reported the preparation of NiS/g-C<sub>3</sub>N<sub>4</sub> *via* ion exchange that converts Ni<sup>2+</sup>/g-C<sub>3</sub>N<sub>4</sub> to NiS/g-C<sub>3</sub>N<sub>4</sub> using Na<sub>2</sub>S.<sup>48</sup> Another type of nickel sulfide supported on g-C<sub>3</sub>N<sub>4</sub>, NiS<sub>2</sub>/g-C<sub>3</sub>N<sub>4</sub>, was prepared *via* a hydrothermal method using NiAc and thiourea in the presence of g-C<sub>3</sub>N<sub>4</sub>.<sup>49</sup> The activity of the optimized NiS<sub>2</sub>/g-C<sub>3</sub>N<sub>4</sub> system is 4 times that of Pt/g-C<sub>3</sub>N<sub>4</sub>. However, the activity dropped to 60% of the initial value after five cycles. All these results indicate that nickel sulfides represent promising cocatalysts for the construction of noble metal free g-C<sub>3</sub>N<sub>4</sub> photocatalysts for hydrogen evolution. In addition, cobalt sulfide has been evaluated as a cocatalyst for mpg-C<sub>3</sub>N<sub>4</sub><sup>47,50</sup> and exhibited lower activities than NiS under the same conditions.<sup>47</sup>

In the family of metal sulfides, MoS<sub>2</sub> and WS<sub>2</sub> nanosheets have received a lot of interests as efficient noble metal free HER catalysts for both electrocatalytic and photocatalytic reactions.<sup>51</sup> MoS<sub>2</sub> and WS<sub>2</sub> have also been loaded on g-C<sub>3</sub>N<sub>4</sub> to act as cocatalysts. It is expected that the nanosheet morphology of these catalysts can facilitate charge transfer between

g-C<sub>3</sub>N<sub>4</sub> and the catalyst. Furthermore, the thin layer structure of the nanosheets can minimize the light blocking effect by cocatalysts in the aggregated form. Both MoS<sub>2</sub>/mpg-C<sub>3</sub>N<sub>4</sub> and WS<sub>2</sub>/mpg-C<sub>3</sub>N<sub>4</sub> were prepared by an impregnation method.<sup>52,53</sup> As schematically shown in Fig. 2A, (NH<sub>4</sub>)<sub>2</sub>MoS<sub>4</sub> or (NH<sub>4</sub>)<sub>2</sub>WS<sub>4</sub> was impregnated on mpg-C<sub>3</sub>N<sub>4</sub> and the subsequent sulfidation was carried out in H<sub>2</sub>S or H<sub>2</sub>S/H<sub>2</sub> atmosphere at an elevated temperature. MoS<sub>2</sub> nanosheets were observed in HRTEM images (Fig. 2B). As can be seen in Fig. 2C, the activity of the optimized MoS<sub>2</sub>/mpg-C<sub>3</sub>N<sub>4</sub> was found to be higher than that of Pt/mpg-C<sub>3</sub>N<sub>4</sub> and a QE of 2.1% was obtained at 400 nm. The stability of this system is also good with 80% of the initial activity maintained after recycling for four runs. Compared to MoS<sub>2</sub>/mpg-C<sub>3</sub>N<sub>4</sub>, the activity of WS<sub>2</sub>/mpg-C<sub>3</sub>N<sub>4</sub> is relatively lower and decreased dramatically after recycle runs.

Hydroxides such as Ni(OH)<sub>2</sub> and Cu(OH)<sub>2</sub> were also reported to be capable of evolving hydrogen when coupled with g-C<sub>3</sub>N<sub>4</sub>.<sup>54,55</sup> The preparation method of hydroxide/g-C<sub>3</sub>N<sub>4</sub> was simply precipitating metal cations by NaOH with pre-added g-C<sub>3</sub>N<sub>4</sub> followed by aging for a certain period of time. Both Ni(OH)<sub>2</sub>/g-C<sub>3</sub>N<sub>4</sub> and Cu(OH)<sub>2</sub>/g-C<sub>3</sub>N<sub>4</sub> were found to be stable and efficient for photocatalytic hydrogen production. A relatively high QE of 1.1% was obtained over Ni(OH)<sub>2</sub>/g-C<sub>3</sub>N<sub>4</sub> at 420 nm. XPS study for the hydroxide/g-C<sub>3</sub>N<sub>4</sub> samples before and after photoreaction revealed that the *in situ* formed Ni<sup>0</sup> or Cu<sup>0</sup> cluster *via* reduction of metal ions by photo electrons is the key to the hydrogen production process.

Very recently, Zhang *et al.* prepared a core-shell structured Ni/NiO loaded on g-C<sub>3</sub>N<sub>4</sub> by an impregnation method for hydrogen production.<sup>56</sup> Ni<sup>2+</sup> on g-C<sub>3</sub>N<sub>4</sub> was first reduced to Ni nanoparticles in H<sub>2</sub> flow and then the surface of the Ni nanoparticles was oxidized to NiO after being annealed in air leading to the formation of core-shell nanostructure. Ni/NiO-g-C<sub>3</sub>N<sub>4</sub> showed improved activity for photocatalytic hydrogen production compared with the pristine g-C<sub>3</sub>N<sub>4</sub>, Ni-g-C<sub>3</sub>N<sub>4</sub> and NiO-g-C<sub>3</sub>N<sub>4</sub> due to the enhanced charge transfer across the interface. The overpotential for HER was also reduced for Ni/NiO-g-C<sub>3</sub>N<sub>4</sub>, confirming that the Ni/NiO core/shell structure is a suitable catalyst for HER.

In short, various noble metal free g-C<sub>3</sub>N<sub>4</sub> based photocatalysts have been investigated. It is promising to find that the activities of some photocatalysts approach or surpass that of Pt/g-C<sub>3</sub>N<sub>4</sub>. However, it is still challenging to prepare stable and efficient noble metal free g-C<sub>3</sub>N<sub>4</sub> photocatalysts with their activities comparable or better than other semiconductor based systems. The photoelectric current and photocatalytic efficiency are still low due to the drawbacks mentioned before. One of the possible solutions could be the development of new preparation methods to enhance the interface between the cocatalysts and g-C<sub>3</sub>N<sub>4</sub>. Furthermore, similar to the case of graphene, the electronic and morphological properties of g-C<sub>3</sub>N<sub>4</sub> itself could be tuned by exfoliation to enhance the photocatalytic performances, which is discussed in the next section.

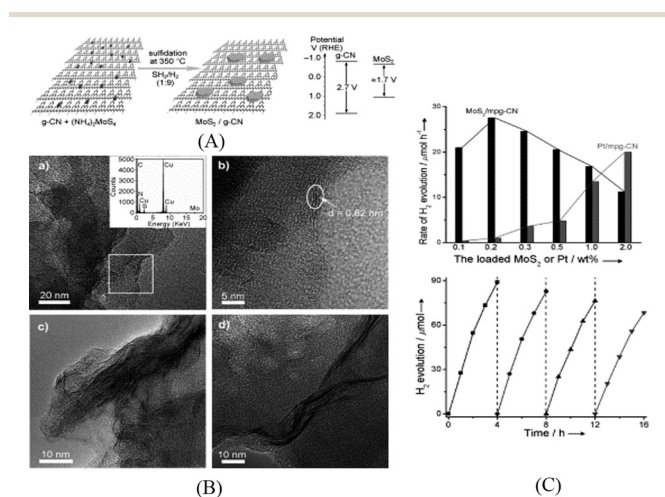


Fig. 2 (A) Schematic of the MoS<sub>2</sub>/mpg-C<sub>3</sub>N<sub>4</sub> nanojunction and the band energy diagram; (B) TEM and HRTEM images of MoS<sub>2</sub>/mpg-C<sub>3</sub>N<sub>4</sub>; (C) hydrogen production rate of mpg-C<sub>3</sub>N<sub>4</sub> loaded with MoS<sub>2</sub> or Pt and recycling behavior for 0.2 wt% MoS<sub>2</sub>/mpg-C<sub>3</sub>N<sub>4</sub>.<sup>52</sup> Copyright 2013 WILEY-VCH Verlag GmbH & Co. KGaA Weinheim.



### 3. Generation of g-C<sub>3</sub>N<sub>4</sub> nanosheets by exfoliation toward enhanced photocatalytic activity

Among various methods for control and modification of the morphology of g-C<sub>3</sub>N<sub>4</sub>, exfoliation is a simple and facile process which has been shown effective to enhance the photocatalytic performance of g-C<sub>3</sub>N<sub>4</sub>. Bulk g-C<sub>3</sub>N<sub>4</sub> has a graphite-like structure which contains elementary layers built up from the ring structure of carbon nitride and van der Waals interaction between the layers. This unique structure makes g-C<sub>3</sub>N<sub>4</sub> possible to be exfoliated into graphene-like single layered nanosheets. By exfoliating bulk g-C<sub>3</sub>N<sub>4</sub> into nanosheets, the specific surface area can be increased and the catalytic centers are exposed. Furthermore, due to the quantum confinement effect, the conduction band (CB) position of g-C<sub>3</sub>N<sub>4</sub> nanosheets can be shifted to more negative values than that of their bulk compartment, which provides a larger driving force for photocatalytic reaction.

The exfoliation methods of g-C<sub>3</sub>N<sub>4</sub> can be classified as thermal exfoliation and liquid exfoliation. Niu *et al.* reported the preparation of graphene-like g-C<sub>3</sub>N<sub>4</sub> nanosheets by thermal etching of bulk g-C<sub>3</sub>N<sub>4</sub>.<sup>57</sup> After the g-C<sub>3</sub>N<sub>4</sub> sample was thermally oxidized in air at 500 °C for 2 h, g-C<sub>3</sub>N<sub>4</sub> nanosheets with a thickness ranging from 1.62 nm to 2.62 nm were obtained corresponding to 4 to 7 carbon nitride layers. Compared to bulk g-C<sub>3</sub>N<sub>4</sub>, the optical absorption of g-C<sub>3</sub>N<sub>4</sub> nanosheets exhibited a 20 nm blue shift which is due to quantum confinement. The surface area of g-C<sub>3</sub>N<sub>4</sub> nanosheets increased from 50 m<sup>2</sup> g<sup>-1</sup> to 306 m<sup>2</sup> g<sup>-1</sup>. The synergistic effect of the higher surface area and the more negative CB position results in a significant increase in their hydrogen production activity. Xu *et al.* further modified this thermal exfoliation method by firstly preparing an NH<sub>4</sub>Cl/g-C<sub>3</sub>N<sub>4</sub> composite with NH<sub>4</sub>Cl intercalated in the interlayer space *via* hydrothermal reaction. Then the composite was annealed in N<sub>2</sub> to exfoliate g-C<sub>3</sub>N<sub>4</sub> into nanosheets by the evolved gaseous NH<sub>3</sub>.<sup>58</sup> The preparation method is schematically illustrated in Fig. 3A. The surface area of g-C<sub>3</sub>N<sub>4</sub> nanosheets is 10 times that of the bulk g-C<sub>3</sub>N<sub>4</sub> prepared using dicyandiamide as the precursor.

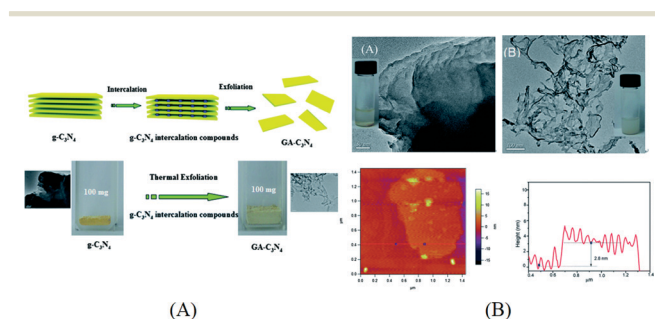


Fig. 3 (A) Schematics of thermal exfoliation of g-C<sub>3</sub>N<sub>4</sub> into nanosheets and optical images of g-C<sub>3</sub>N<sub>4</sub> before and after exfoliation; (B) typical TEM images of bulk g-C<sub>3</sub>N<sub>4</sub> and g-C<sub>3</sub>N<sub>4</sub> nanosheets, AFM image and thickness profile of exfoliated nanosheets. Reproduced from ref. 58 with permission from The Royal Society of Chemistry.

As shown in Fig. 3B, the average thickness of the as-prepared g-C<sub>3</sub>N<sub>4</sub> nanosheets is around 2.8 nm, measured by atomic force microscopy (AFM). Although thermal exfoliation is considered to be a low cost, large scale and environmentally friendly method for preparing g-C<sub>3</sub>N<sub>4</sub> nanosheets, the highest yield of the nanosheets obtained so far is 6 wt% of the starting bulk g-C<sub>3</sub>N<sub>4</sub>.<sup>57</sup>

Liquid exfoliation is a more commonly used method and is done by ultrasonication of bulk g-C<sub>3</sub>N<sub>4</sub> in a suitable solvent. After this process, the exfoliated nanosheets can be easily separated from the remaining bulk g-C<sub>3</sub>N<sub>4</sub> by centrifugation. It is considered as a facile method for the preparation of 2D materials. Zhang *et al.* firstly reported the preparation of g-C<sub>3</sub>N<sub>4</sub> nanosheets using water as the solvent during ultrasonication.<sup>59</sup> As there is dangling hydrogen in the carbon nitride layer of g-C<sub>3</sub>N<sub>4</sub>, it was supposed that a polar solvent like H<sub>2</sub>O is effective for the swelling and exfoliation of g-C<sub>3</sub>N<sub>4</sub>. The swelling and exfoliation process is shown in Fig. 4A. Besides H<sub>2</sub>O, formamide, dimethylformamide, ethanol and methanol were used as exfoliation solvents. Only H<sub>2</sub>O was found effective and the concentration of the resulting nanosheet suspension was measured to be 0.15 mg mL<sup>-1</sup>. The change in UV-vis spectrum and photoluminescence (PL) spectrum before and after exfoliation can be attributed to the enlarged bandgap induced by quantum confinement (Fig. 4B). As shown in Fig. 4C, the thickness of the as-prepared g-C<sub>3</sub>N<sub>4</sub> nanosheets is ~2.5 nm, corresponding to 7 atomic layers, and the lateral length of the nanosheets ranges from 70 nm to 140 nm. The as-prepared nanosheets were used for bioimaging due to their high PL quantum yield and biocompatibility. Inspired by this result, researchers have adopted the liquid exfoliation method for the preparation of g-C<sub>3</sub>N<sub>4</sub> nanosheets and expanded the application of g-C<sub>3</sub>N<sub>4</sub> nanosheets to other areas. For example, Sun and co-workers applied the same method and used the resulting nanosheets as an efficient fluoro-sensor for detection of Cu<sup>2+</sup>.<sup>60</sup> Cheng *et al.* exfoliated g-C<sub>3</sub>N<sub>4</sub> in water and loaded Au nanoparticles on the exfoliated g-C<sub>3</sub>N<sub>4</sub> nanosheets *via* photodeposition. The composite was found to be able to efficiently degrade methyl orange under visible light.<sup>61</sup> In addition, Zhang *et al.*

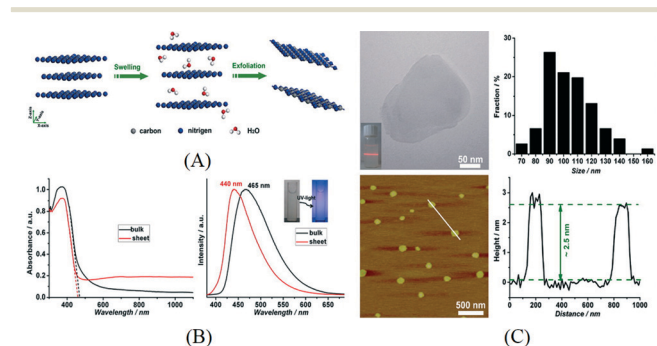


Fig. 4 (A) Schematics of the swelling and exfoliation of g-C<sub>3</sub>N<sub>4</sub> by H<sub>2</sub>O; (B) UV-vis spectrum and PL spectrum for bulk g-C<sub>3</sub>N<sub>4</sub> and nanosheets; (C) typical TEM image and AFM image showing the lateral dimensions and thickness of g-C<sub>3</sub>N<sub>4</sub> nanosheets. Reprinted with permission from ref. 59. Copyright 2015 American Chemical Society.



reported that the reaction pathway for photocatalytic phenol degradation is changed when exfoliated nanosheets were used as the photocatalyst.<sup>62</sup> In this case, g-C<sub>3</sub>N<sub>4</sub> nanosheets with a thickness of 2 nm were prepared by sonication in water. The change in bandgap and CB position was measured by the UV-vis spectrum and Mott-Schottky plot. It was found that oxygen was reduced to H<sub>2</sub>O<sub>2</sub> on g-C<sub>3</sub>N<sub>4</sub> nanosheets *via* a two-electron transfer process while 'O<sub>2</sub><sup>-</sup>' was formed on the surface of bulk g-C<sub>3</sub>N<sub>4</sub> *via* a one-electron transfer process. This was attributed to the formation of 1,4-endoperoxide species on the surface of g-C<sub>3</sub>N<sub>4</sub> nanosheets. The two-electron transfer pathway promoted the efficient separation of excited electrons and holes and facilitated the formation of reactive species which resulted in the enhanced photocatalytic activity for phenol degradation.

Besides water, other polar solvents or mixed solvents have also been investigated for the exfoliation of g-C<sub>3</sub>N<sub>4</sub>. For instance, isopropanol alcohol (IPA) was found to be another suitable solvent for exfoliation of g-C<sub>3</sub>N<sub>4</sub> into nanosheets due to the surface energy matching of IPA and g-C<sub>3</sub>N<sub>4</sub>.<sup>63</sup> An extended sonication duration of 10 h yielded g-C<sub>3</sub>N<sub>4</sub> nanosheets with an average thickness of 2 nm which is thinner than those prepared using H<sub>2</sub>O as the solvent. Similarly, the exfoliated g-C<sub>3</sub>N<sub>4</sub> nanosheets exhibited a high surface area of 384 m<sup>2</sup> g<sup>-1</sup>. The electrochemical impedance spectrum (EIS) results indicated an enhanced charge separation and transfer ability. Compared to bulk g-C<sub>3</sub>N<sub>4</sub>, the electron transfer resistance of g-C<sub>3</sub>N<sub>4</sub> nanosheets decreased by 75%. The photocatalytic hydrogen production activity of g-C<sub>3</sub>N<sub>4</sub> nanosheets is 10 times that of the bulk counterpart and is also higher than that of mpg-C<sub>3</sub>N<sub>4</sub>. In another work, She *et al.* prepared g-C<sub>3</sub>N<sub>4</sub> nanosheets *via* sonication in 1,3-butanediol (1,3-BUT).<sup>64</sup> Due to the polarity and surface energy matching, 1,3-BUT can swell and exfoliate g-C<sub>3</sub>N<sub>4</sub> into nanosheets with a thickness of 0.9–2.1 nm. Mixed solvents have also been used for exfoliation of g-C<sub>3</sub>N<sub>4</sub> such as the mixture of ethanol and water.<sup>65</sup> Interestingly, it was found that the ratio of the two solvents affects the yield and the highest concentration of nanosheets at 3 mg mL<sup>-1</sup> was obtained with an ethanol/water volume ratio of 1 : 3. This concentration is much higher than that obtained in the single solvent. Furthermore, it is usual that a g-C<sub>3</sub>N<sub>4</sub> monolayer was obtained using such mixed solvents. Monolayer g-C<sub>3</sub>N<sub>4</sub> nanosheets can also be produced *via* a combination of heat treatment and liquid exfoliation and the resultant nanosheets exhibited efficient photocatalytic disinfection activity for *Escherichia coli*.<sup>66</sup> Fig. 5 shows the EIS curves and transient photoresponse of the bulk and single-layered g-C<sub>3</sub>N<sub>4</sub>, indicating the enhanced charge transportation properties of the g-C<sub>3</sub>N<sub>4</sub> nanosheets.

Although facile and simple, the disadvantage of liquid exfoliation method is obvious. It usually takes long sonication time and the yield is generally lower than 15%. In our recent work, the exfoliation of mpg-C<sub>3</sub>N<sub>4</sub> in ethanol was carried out using a probe sonicator.<sup>67</sup> The probe sonicator with a higher power intensity is directly immersed into the suspension and hence is much more effective than a bath sonicator. It is widely

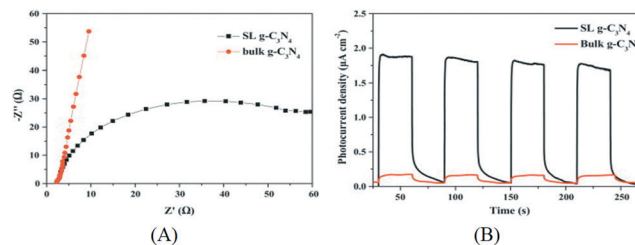


Fig. 5 (A) EIS of the bulk g-C<sub>3</sub>N<sub>4</sub> and single-layered g-C<sub>3</sub>N<sub>4</sub>; (B) transient photoresponse of bulk g-C<sub>3</sub>N<sub>4</sub> and single-layered g-C<sub>3</sub>N<sub>4</sub>. Reprinted from ref. 65, copyright 2015 with permission from Elsevier.

used in the exfoliation of layered metal chalcogenides like MoS<sub>2</sub>.<sup>68</sup> The resultant yield (25.8%) for exfoliated mpg-C<sub>3</sub>N<sub>4</sub> nanosheets was much higher than previously reported values. As shown in Fig. 6A, the thickness of such mpg-C<sub>3</sub>N<sub>4</sub> nanosheets was 2–3 nm in average, corresponding to 5–8 carbon nitride layers. After depositing Pt or Co<sub>3</sub>O<sub>4</sub> on the surface of mpg-C<sub>3</sub>N<sub>4</sub> nanosheets as a cocatalyst (Fig. 6B), the photocatalytic activities for hydrogen evolution or degradation of Rhodamine B, respectively, were greatly enhanced compared to those of the bulk g-C<sub>3</sub>N<sub>4</sub> (Fig. 6C and D). It is remarkable that the hydrogen evolution rate is 26 times that of the bulk g-C<sub>3</sub>N<sub>4</sub>.

Inspired by the Hummers method for the exfoliation of graphite into graphene, Zhu *et al.* developed a chemical etching method for the preparation of single atomic layered g-C<sub>3</sub>N<sub>4</sub> nanosheets.<sup>69</sup> It was found that only nanoparticles were obtained in the presence of KMnO<sub>4</sub> since g-C<sub>3</sub>N<sub>4</sub> is not stable enough against oxidation by KMnO<sub>4</sub>.<sup>57</sup> H<sub>2</sub>SO<sub>4</sub> (98%) was firstly intercalated into the interlayer space of g-C<sub>3</sub>N<sub>4</sub>. Then g-C<sub>3</sub>N<sub>4</sub> nanosheets were obtained by the rapid heating

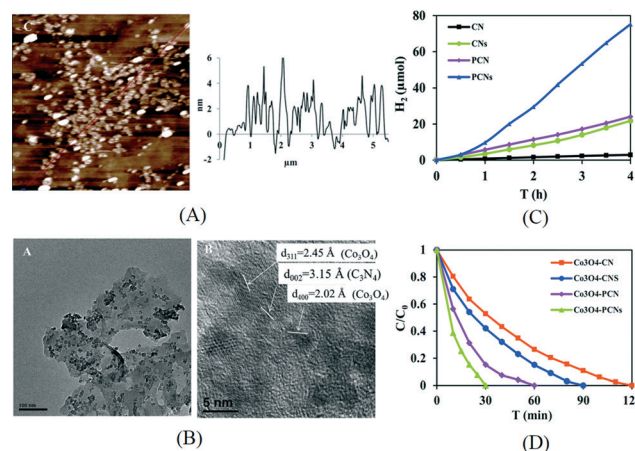


Fig. 6 (A) AFM image and thickness profile of mpg-C<sub>3</sub>N<sub>4</sub> nanosheets exfoliated using a probe sonicator; (B) TEM and HRTEM images of Co<sub>3</sub>O<sub>4</sub>/porous g-C<sub>3</sub>N<sub>4</sub> nanosheets; (C) hydrogen production over Pt loaded g-C<sub>3</sub>N<sub>4</sub> samples under visible light; (D) degradation of Rhodamine B over Co<sub>3</sub>O<sub>4</sub> loaded g-C<sub>3</sub>N<sub>4</sub> samples under UV-vis light (CN: g-C<sub>3</sub>N<sub>4</sub>, CNS: exfoliated g-C<sub>3</sub>N<sub>4</sub> nanosheets, PCN: mesoporous g-C<sub>3</sub>N<sub>4</sub>, PCNs: exfoliated mesoporous g-C<sub>3</sub>N<sub>4</sub> nanosheets). Reproduced from ref. 67 with permission from The Royal Society of Chemistry.



effect of  $\text{H}_2\text{SO}_4$  (98%) mixed with water. The yield of  $\text{g-C}_3\text{N}_4$  nanosheets reached as high as 30%. AFM observation revealed that the thickness of 60% of the exfoliated nanosheets was around 0.4 nm, which is close to the theoretical thickness of a single carbon nitride layer. Correspondingly, the surface area was significantly increased from  $4.3 \text{ m}^2 \text{ g}^{-1}$  to  $205.8 \text{ m}^2 \text{ g}^{-1}$  after exfoliation. After loading Pt on the surface of the as-prepared  $\text{g-C}_3\text{N}_4$  nanosheets, they exhibited an enhancement factor of 2.6 for hydrogen evolution compared to bulk  $\text{g-C}_3\text{N}_4$ . A subsequent research work demonstrated that the surface charge of the nanosheets prepared using this chemical etching method can be tuned by adding a different charge guest. The electrostatic assembly of the  $\text{g-C}_3\text{N}_4$  nanosheets with CdS or BiOBr was prepared and investigated for the photocatalytic degradation of methyl orange (MO) and aminobenzoic acid.<sup>70</sup> The CdS/ $\text{g-C}_3\text{N}_4$  nanosheet composite exhibited superior photocatalytic activity. However, before the nanosheets can be used for photocatalytic reaction, the suspension should be carefully and thoroughly washed to fully remove the acid.

Besides the abovementioned research efforts, the exfoliated  $\text{g-C}_3\text{N}_4$  nanosheets have also been coupled with other materials such as carbon nanotubes, reduced graphene oxide and  $\text{WO}_3$  arrays *via* electrostatic interactions for potential application in electrocatalysis or PEC reactions.<sup>71–74</sup> In summary,  $\text{g-C}_3\text{N}_4$  can be effectively exfoliated into monolayer or few layered nanosheets in polar solvents including water, some organic solvents and acid solution, or by a simple thermal exfoliation. The exfoliated nanosheets present enhanced photocatalytic or PEC activities due to the larger specific surface area, enhanced charge separation and transfer ability and more negative CB. The exfoliation process is simple but time consuming and the yield of nanosheets is generally low. Another main disadvantage of the sonication assisted exfoliation method is that boundary defects may be induced during the treatment which may lead to charge recombination. So far, we are unable to synthesize larger domain sizes with the current synthetic scheme.<sup>12</sup> Further development of efficient and economic preparation methods for  $\text{g-C}_3\text{N}_4$  nanosheets is needed for their practical applications.

## 4. $\text{g-C}_3\text{N}_4$ based photocatalysts for oxygen evolution and overall water splitting

Water oxidation, the other half reaction in overall water splitting, is a four-electron transfer process and considered to be the rate-limiting step in overall water splitting. Most of the research efforts on  $\text{g-C}_3\text{N}_4$  based photocatalysts have been focused on the water reduction half reaction, which proceeds in the presence of a hole scavenger. There are only limited studies on water oxidation by the  $\text{g-C}_3\text{N}_4$  system, not to mention overall water splitting. Despite the energetic barrier and sluggish kinetics, water oxidation by  $\text{g-C}_3\text{N}_4$  also suffers from the self-oxidation of the catalyst which leads to the evolution

of  $\text{N}_2$  similar to the case of (oxy)nitrides *e.g.*  $\text{Ta}_3\text{N}_5$  and  $\text{LaTiO}_2\text{N}$ .<sup>75</sup> An efficient cocatalyst and a protection layer need to be developed to mitigate this problem.

When  $\text{g-C}_3\text{N}_4$  was first reported to be active for water splitting, its oxygen evolution activity was studied using  $\text{AgNO}_3$  as an electron acceptor.<sup>11</sup> With  $\text{RuO}_2$  loaded as a water oxidation catalyst (WOC),  $\text{g-C}_3\text{N}_4$  was shown to be able to oxidize water into  $\text{O}_2$  with a low reaction rate. Maeda *et al.* showed that photocorrosion can be significantly inhibited by loading  $\text{RuO}_2$  as an efficient WOC. Otherwise the evolution of  $\text{N}_2$  is significant.<sup>76</sup> When the loading amount of  $\text{RuO}_2$  was optimized to 3 wt%, the highest oxygen evolution rate was obtained ( $12 \mu\text{mol h}^{-1}$ ). McMillan *et al.* studied the effect of the precursor and reaction parameters during  $\text{g-C}_3\text{N}_4$  preparation on its oxygen evolution activity with  $\text{RuO}_2$  as the cocatalyst.<sup>77</sup>

Besides the aforementioned drawbacks of  $\text{g-C}_3\text{N}_4$ , one of the main factors limiting its water oxidation activity is its VB edge position at about 1.4 V *vs.* NHE.<sup>11,14,15</sup> Compared to the VB position of widely studied oxides such as  $\text{WO}_3$  (2.7 V *vs.* NHE),  $\text{BiVO}_4$  (2.8 V *vs.* NHE) and  $\text{Fe}_2\text{O}_3$  (2.2 V *vs.* NHE),  $\text{g-C}_3\text{N}_4$  can only provide moderate water oxidation ability.<sup>78</sup> Wang and co-workers used trithiocyanuric acid as the precursor to prepare sulfur-mediated  $\text{g-C}_3\text{N}_4$  (CNS).<sup>79</sup> After condensation, the sulfur amount in the final product was less than 1 wt%. The release of sulfur species during synthesis altered the connectivity pattern as well as the topology of  $\text{g-C}_3\text{N}_4$  and lowered the VB position by *ca.* 0.2 V. It showed a 4-fold increase in  $\text{O}_2$  production compared to the pristine  $\text{g-C}_3\text{N}_4$ . However, the oxygen production rate of CNS was only  $2.5 \mu\text{mol h}^{-1}$  under visible light irradiation since the photocatalytic experiment was conducted without loading a suitable WOC.

Then, the same group loaded cobalt species as WOC on CNS by an impregnation method and constructed an efficient noble metal free photocatalysis system for water oxidation.<sup>80</sup> The structure of the cocatalyst was confirmed to be mainly  $\text{Co}_3\text{O}_4$  by XPS and HRTEM. Fluorescence quenching study indicated efficient charge transfer from CNS to  $\text{Co}_3\text{O}_4$ . The PEC study showed that  $\text{Co}_3\text{O}_4/\text{CNS}$  lowered the onset potential of anodic photocurrent by 120 mV and also enhanced the photocurrent response. Using  $\text{AgNO}_3$  as an electron acceptor, the optimized  $\text{Co}_3\text{O}_4/\text{CNS}$  exhibited an oxygen evolution rate of  $25.1 \mu\text{mol h}^{-1}$  under visible light. However, the oxygen evolution rate gradually decreased after 5 h which could be due to the deposition of Ag nanoparticles which blocked the catalytic centers as well as light absorption. Recently, Zhang *et al.* reported the deposition of another cobalt-based cocatalyst,  $\text{Co(OH)}_2$ , on the surface of  $\text{g-C}_3\text{N}_4$  *via* simple precipitation (Fig. 7A). The PL quenching study in Fig. 7B revealed the efficient charge transfer from  $\text{g-C}_3\text{N}_4$  to  $\text{Co(OH)}_2$ . During the first hour, the oxygen evolution rate obtained was  $27.4 \mu\text{mol h}^{-1}$  under UV-vis light irradiation (Fig. 7C).<sup>81</sup> After calcination in air,  $\text{Co(OH)}_2/\text{g-C}_3\text{N}_4$  can be converted to  $\text{Co}_3\text{O}_4/\text{g-C}_3\text{N}_4$ , which is less active. Furthermore, the electrocatalytic oxygen evolution reaction (OER) onset potential of  $\text{Co(OH)}_2/\text{g-C}_3\text{N}_4$



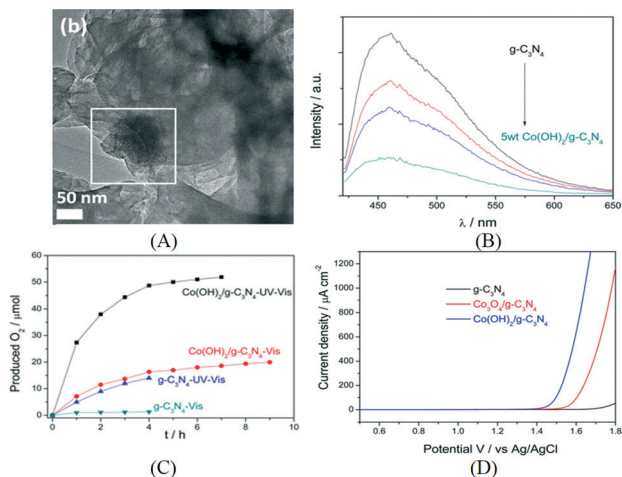


**Fig. 7** (A) TEM image of  $\text{Co(OH)}_2/\text{g-C}_3\text{N}_4$ ; (B) PL quenching of  $\text{g-C}_3\text{N}_4$  and  $\text{Co(OH)}_2/\text{g-C}_3\text{N}_4$ ; (C) photocatalytic oxygen production over  $\text{g-C}_3\text{N}_4$  and  $\text{Co(OH)}_2/\text{g-C}_3\text{N}_4$  under different conditions; (D) linear sweep voltammogram of different samples. Reprinted with permission from ref. 81. Copyright 2015 American Chemical Society.

was found to be lower than that of  $\text{Co}_3\text{O}_4/\text{g-C}_3\text{N}_4$  by the linear sweep voltammogram shown in Fig. 7D.

In the area of overall water splitting by  $\text{g-C}_3\text{N}_4$  based systems, only limited literature has been found reporting the successful construction of  $\text{g-C}_3\text{N}_4$  photocatalysts that can evolve  $\text{H}_2$  and  $\text{O}_2$  simultaneously at a stoichiometric ratio. Lee *et al.* decorated a cobalt phosphate ( $\text{CoPi}$ ) catalyst on the surface of  $\text{mpg-C}_3\text{N}_4$  via direct photodeposition of  $\text{Co}^{2+}$  ions in a phosphate buffer solution or first deposition of metallic cobalt nanoparticles and then conversion of metallic nanoparticles to  $\text{CoPi}$  on  $\text{mpg-C}_3\text{N}_4$ .<sup>82</sup> The as-prepared  $\text{CoPi}/\text{mpg-C}_3\text{N}_4$  is active for both HER and OER half reactions in the presence of a suitable hole and electron scavenger, respectively.  $\text{CoPi}$ , a widely studied OER catalyst, was found to be converted *in situ* to Co-oxo/hydroxo-phosphate which is an active electrocatalyst for HER when a hole scavenger exists. In the absence of any charge scavenger,  $\text{CoPi}/\text{mpg-C}_3\text{N}_4$  was found to be able to split water into  $\text{H}_2$  and  $\text{O}_2$  at a stoichiometric ratio in phosphate buffer solution with  $\text{H}_2$  and  $\text{O}_2$  produced at  $13.6 \mu\text{mol g}^{-1} \text{h}^{-1}$  and  $6.6 \mu\text{mol g}^{-1} \text{h}^{-1}$ , respectively. The activity for overall water splitting is stable after three runs. Though the reaction rate is still very low, this is the first example of overall water splitting by a  $\text{g-C}_3\text{N}_4$  based photocatalyst.

Besides the single particulate system described earlier, using a Z-scheme photocatalyst which contains two photon systems is another way to achieve overall water splitting. Inspired by natural photosynthesis, the Z-scheme system is composed of a  $\text{H}_2$ -evolving photocatalyst, an  $\text{O}_2$ -evolving photocatalyst and an electron mediator. Photocatalysts that are only active for half reactions can be employed to construct Z-scheme systems, which extends the choice of photocatalyst for overall water splitting. However, the activity of a Z-scheme system depends highly on a suitable combination of its components. So far the most active Z-scheme system

employs  $\text{Ru}/\text{SrTiO}_3:\text{Rh}$  and  $\text{BiVO}_4$  as the  $\text{H}_2$ -evolving photocatalyst and the  $\text{O}_2$ -evolving photocatalyst, respectively.<sup>83</sup> Other photocatalysts such as metal oxynitrides and metal sulfides are less active or inactive for the Z-scheme system. Tang and his co-workers constructed for the first time a Z-scheme system employing  $\text{g-C}_3\text{N}_4$  as the  $\text{H}_2$ -evolving photocatalyst.<sup>84</sup> The mechanism is illustrated in Fig. 8A. Both  $\text{BiVO}_4$  and  $\text{WO}_3$  were used as the  $\text{O}_2$ -evolving photocatalyst and soluble  $\text{Fe}^{3+}/\text{Fe}^{2+}$  and  $\text{IO}_3^-/\text{I}^-$  pairs were used as the electron mediator. With such a scheme, stoichiometric  $\text{H}_2$  and  $\text{O}_2$  were produced. As shown in Fig. 8,  $\text{g-C}_3\text{N}_4\text{-NaI-WO}_3$  was the most efficient in this Z-scheme configuration with production rates of  $\text{H}_2$  and  $\text{O}_2$  at  $74 \mu\text{mol g}^{-1} \text{h}^{-1}$  and  $37 \mu\text{mol g}^{-1} \text{h}^{-1}$ , respectively, under full arc irradiation. The stability of this system is also confirmed to be good as stoichiometric  $\text{H}_2$  and  $\text{O}_2$  are evolved after three recycling runs and the gas production rate is almost the same as the initial run (Fig. 8D). Very recently, an effort was made on the construction of a mediator free Z-scheme overall water splitting system using  $\text{g-C}_3\text{N}_4$  and  $\text{WO}_3$  as the HER and OER photocatalysts, respectively.<sup>85</sup> The  $\text{g-C}_3\text{N}_4\text{-WO}_3$  composite was synthesized by *in situ* growth of  $\text{WO}_3$  on the surface of  $\text{g-C}_3\text{N}_4$  in a hydrothermal reaction. In addition, they used reduced graphene oxide (rGO) as the electron mediator which is expected to enhance the performance. After loading Pt as the cocatalyst, the photoactivity of  $\text{g-C}_3\text{N}_4\text{-WO}_3$  and  $\text{g-C}_3\text{N}_4/\text{rGO-WO}_3$  was measured in pure water without redox couples such as  $\text{I}^-/\text{IO}_3^-$ . Stoichiometric  $\text{H}_2$  and  $\text{O}_2$  can be stably evolved under visible light irradiation. A QE of 0.9% was obtained with the optimized sample at 420 nm. These results indicate that the intimate contact between two photocatalysts and improved electron transfer ability may benefit the  $\text{H}_2/\text{O}_2$  evolution in the two step

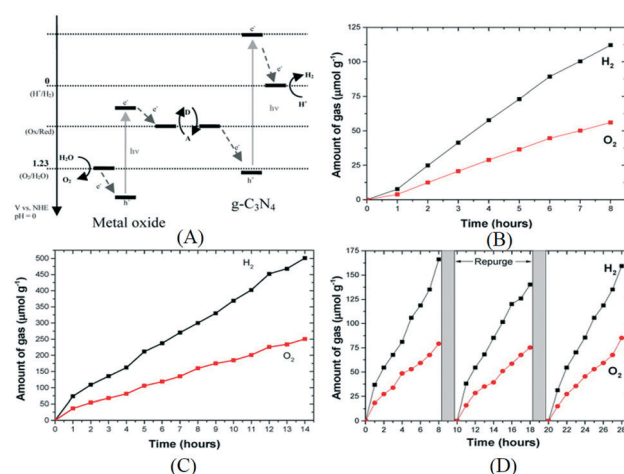


**Fig. 8** (A) Schematics of Z-scheme photocatalysts constructed using  $\text{g-C}_3\text{N}_4$  as the  $\text{H}_2$ -evolving photocatalyst and metal oxides as the  $\text{O}_2$ -evolving photocatalyst; overall water splitting over (B)  $\text{g-C}_3\text{N}_4\text{-FeCl}_2\text{-BiVO}_4$  under full arc irradiation, (C)  $\text{g-C}_3\text{N}_4\text{-NaI-WO}_3$  under full arc irradiation, (D)  $\text{g-C}_3\text{N}_4\text{-NaI-WO}_3$  under visible light irradiation. Reprinted with permission from ref. 84. Copyright 2015 American Chemical Society.



photoexcitation Z-scheme system. Further improvement of the activity of these systems is still needed.

Recently, Kang *et al.* constructed a metal free g-C<sub>3</sub>N<sub>4</sub> based composite photocatalyst by coupling g-C<sub>3</sub>N<sub>4</sub> with carbon dots (CDs).<sup>86</sup> The solar to hydrogen (STH) efficiency reached 2% for the optimized CDs/g-C<sub>3</sub>N<sub>4</sub> system, which is much higher than the thus reported values for photocatalytic systems except that of CoO (5.1%) which is self-corroded within 1 h.<sup>87</sup> Such an STH efficiency reaches not far from the value of 5% set by the U.S. Department of Energy, which corresponds to the H<sub>2</sub> production cost of \$2.3 per kg. Furthermore CD/g-C<sub>3</sub>N<sub>4</sub> exhibited long term stability for 200 days with the catalyst being separated, dried and reused after each day. The high stability can be attributed to its chemical and structure stability. A two-step OER mechanism including H<sub>2</sub>O<sub>2</sub> production and subsequent decomposition of H<sub>2</sub>O<sub>2</sub> to O<sub>2</sub> was found to be key to the high STH efficiency. This two-step pathway was verified by electrochemical study and shown to be faster than the conventional four-electron process. Thus the STH efficiency was increased by accelerating the rate-limiting step of OER.

In summary, the non-noble metal containing g-C<sub>3</sub>N<sub>4</sub> based system is capable of efficiently evolving O<sub>2</sub> and is promising in overall water splitting. The metal free feature of g-C<sub>3</sub>N<sub>4</sub> makes it a promising platform for the construction of low cost photocatalytic systems to further lower the cost of solar fuel production.

## 5. CO<sub>2</sub> reduction using g-C<sub>3</sub>N<sub>4</sub> based photocatalysts

CO<sub>2</sub> reduction is a rapidly developing research area as this technology provides possible solutions to the environmental and energy problems we are facing. Many studies and reviews have been published showing the promising findings in reduction of CO<sub>2</sub> into value added products.<sup>1,3,8,88–91</sup> Similar to the situation in water oxidation and overall water splitting, there have not been extensive studies on CO<sub>2</sub> photoreduction by g-C<sub>3</sub>N<sub>4</sub> based systems. Nevertheless, during the last few years, CO<sub>2</sub> photoreduction using g-C<sub>3</sub>N<sub>4</sub> has received increasing attention due to the interesting properties of g-C<sub>3</sub>N<sub>4</sub> that may offer some opportunities in this area.

In 2012, Dong and co-workers prepared g-C<sub>3</sub>N<sub>4</sub> and porous g-C<sub>3</sub>N<sub>4</sub> by heating melamine or melamine hydrochloride and investigated their photocatalytic CO<sub>2</sub> reduction activity in the presence of water vapor under visible light.<sup>92</sup> Under these reaction conditions, CO was obtained as the reduction product. Subsequently, Mao *et al.* reported the use of g-C<sub>3</sub>N<sub>4</sub> with different microstructures for CO<sub>2</sub> photoreduction in NaOH solution without depositing any cocatalysts.<sup>93</sup> In this work, urea and melamine were used for the preparation of g-C<sub>3</sub>N<sub>4</sub>. It was found that the specific surface area of u-g-C<sub>3</sub>N<sub>4</sub> (39.5 m<sup>2</sup> g<sup>-1</sup>) is much higher than that of m-g-C<sub>3</sub>N<sub>4</sub> (3.7 m<sup>2</sup> g<sup>-1</sup>), which leads to more efficient surface adsorption, better charge separation and improved photoactivity. The CO<sub>2</sub> reduction products over u-g-C<sub>3</sub>N<sub>4</sub> were CH<sub>3</sub>OH and C<sub>2</sub>H<sub>5</sub>OH

while only C<sub>2</sub>H<sub>5</sub>OH was produced over m-g-C<sub>3</sub>N<sub>4</sub>. It is interesting that hydrocarbons were produced by CO<sub>2</sub> reduction over the g-C<sub>3</sub>N<sub>4</sub> system instead of gaseous CO possibly because the reaction was conducted in aqueous solution. However, CH<sub>3</sub>OH or C<sub>2</sub>H<sub>5</sub>OH may be oxidized on the surface of g-C<sub>3</sub>N<sub>4</sub> by *in situ* evolved O<sub>2</sub> during long photoreaction, as indicated by the decreased reaction rate after irradiation beyond 9 h. Tuning the electronic structure of g-C<sub>3</sub>N<sub>4</sub> by doping S into the pristine g-C<sub>3</sub>N<sub>4</sub> can enhance its optical adsorption as well as the CO<sub>2</sub> reduction activity. S doped g-C<sub>3</sub>N<sub>4</sub> was prepared by the condensation of thiourea and the CH<sub>3</sub>OH yield over S doped g-C<sub>3</sub>N<sub>4</sub> is 1.4 times that over the pristine g-C<sub>3</sub>N<sub>4</sub>.<sup>94</sup> To construct more efficient systems, one strategy is to couple the highly active homogeneous catalyst with g-C<sub>3</sub>N<sub>4</sub>. For instance, a Ru complex, *cis,trans*-[Ru{4,4'-(CH<sub>2</sub>PO<sub>3</sub>H<sub>2</sub>)<sub>2</sub>-2,2'-bipyridine}(CO)<sub>2</sub>Cl<sub>2</sub>] (**Ru**) was adsorbed on the surface of mpg-C<sub>3</sub>N<sub>4</sub> with a high surface area of 180 m<sup>2</sup> g<sup>-1</sup>.<sup>95</sup> The **Ru**/mpg-C<sub>3</sub>N<sub>4</sub> was able to reduce CO<sub>2</sub> into formic acid under visible light while a small amount of H<sub>2</sub> and CO was also detected in acetonitrile in the presence of TEOA as the sacrificial reagent. Isotopic measurement results indicated that formic acid entirely came from CO<sub>2</sub> reduction while 77% of the evolved CO originated from the carbonyl ligand unit of the **Ru** catalyst. The detachment of the carbonyl ligand from **Ru** was a slow process and has also been reported in other papers including homogeneous and heterogeneous systems.<sup>96,97</sup> However, the photocatalytic activity of **Ru**/mpg-C<sub>3</sub>N<sub>4</sub> for formic acid production was found to stay almost unchanged even after 5 h of reaction. The **Ru** catalyst after carbonyl ligand detachment was expected to be the active species for CO<sub>2</sub> reduction. Subsequently, the same group studied the effect of the pore-wall structure of mpg-C<sub>3</sub>N<sub>4</sub> and the effect of the **Ru** complex structure on CO<sub>2</sub> photoreduction.<sup>98,99</sup> Based on these results, it is understood that the photoactivity is sensitive to the specific surface area of mpg-C<sub>3</sub>N<sub>4</sub> and is not related to the pore size and volume. Furthermore, introduction of too much meso-porosity results in the shrinkage of mpg-C<sub>3</sub>N<sub>4</sub> walls and leads to activity drop. With -PO<sub>3</sub>H<sub>2</sub> used as the linker group, **RuP**/mpg-C<sub>3</sub>N<sub>4</sub> efficiently reduced CO<sub>2</sub> to HCOOH under visible light in *N,N*-dimethylacetamide with TEOA as the sacrificial reagent. This hybrid material gave a high turnover number (TON) of larger than 1000 and a QE of 5.7% at 400 nm. In another study, Lin *et al.* prepared a Co(bpy)<sub>3</sub>Cl<sub>2</sub>/g-C<sub>3</sub>N<sub>4</sub> hybrid material by self-assembly as the photocatalyst for the reduction of CO<sub>2</sub> in acetonitrile under visible light in the presence of TEOA.<sup>100</sup> CO and H<sub>2</sub> were the main products. A TON of 4.3 with a relatively high selectivity of 88.4% for CO production was obtained by the optimized hybrid system. The surface of g-C<sub>3</sub>N<sub>4</sub> or mpg-C<sub>3</sub>N<sub>4</sub> was also modified with cobalt species as oxidative promoters to enhance CO<sub>2</sub> photoreduction. Co(bpy)<sub>3</sub>Cl<sub>2</sub>/CoO<sub>x</sub>/mpg-C<sub>3</sub>N<sub>4</sub> gave the highest TON of 13 and the selectivity of CO to H<sub>2</sub> is 78.5%. Noble metal cocatalyst-loaded g-C<sub>3</sub>N<sub>4</sub> has also been used for CO<sub>2</sub> photoreduction. Under UV-vis light, CO<sub>2</sub> can be reduced to hydrocarbons (mainly CH<sub>4</sub>, CH<sub>3</sub>OH and HCHO) using a Pt/g-C<sub>3</sub>N<sub>4</sub> photocatalyst.<sup>101</sup> Pt acts as an



electron sink to enrich the surface of  $g\text{-C}_3\text{N}_4$  with electrons for efficient  $\text{CO}_2$  reduction. The maximum yield can be obtained when the loading amount of Pt was 0.75%. However, Pt can also act as a catalyst for oxidation of HCHO over time. Pt/ $g\text{-C}_3\text{N}_4$  was also prepared *via* a polyol process and used for photoreduction of  $\text{CO}_2$  in the presence of water vapor under day light lamp irradiation.<sup>102</sup>  $\text{CH}_4$  was the main product for  $\text{CO}_2$  reduction and a 5.1 fold enhancement of  $\text{CH}_4$  production was obtained after 2% Pt was loaded on  $g\text{-C}_3\text{N}_4$ .

The composites of  $g\text{-C}_3\text{N}_4$  and metal oxides have been investigated by various research groups for  $\text{CO}_2$  photoreduction. As in the case of hydrogen production, coupling  $g\text{-C}_3\text{N}_4$  with a suitable semiconductor enhances the charge separation *via* band alignment, which leads to increased activity. For example, the composite of  $\text{NaNbO}_3$  nanowires and  $g\text{-C}_3\text{N}_4$  was prepared by annealing the mixture of  $\text{NaNbO}_3$  nanowires and melamine at 520 °C in air.<sup>103</sup> In this case,  $g\text{-C}_3\text{N}_4$  was expected to grow on the surface of  $\text{NaNbO}_3$  and thus to make a good interface, which is revealed by the SEM and TEM images in Fig. 9B and C. The band energy diagram of  $\text{NaNbO}_3$  and  $g\text{-C}_3\text{N}_4$  is shown in the schematics in Fig. 9A. The suitable band alignment between  $\text{NaNbO}_3$  and  $g\text{-C}_3\text{N}_4$  facilitates the charge separation in the composite. After photodeposition of 0.5% Pt, the composite was capable to reduce  $\text{CO}_2$  to  $\text{CH}_4$  and the activity was much higher than those of the individual components loaded with Pt. Cao *et al.* prepared an  $\text{In}_2\text{O}_3/g\text{-C}_3\text{N}_4$  photocatalyst by a solvothermal method in dimethyl sulfoxide.<sup>104</sup>  $\text{In}_2\text{O}_3$  nanocrystals were grown on the surface of sheet-like  $g\text{-C}_3\text{N}_4$ .  $\text{In}_2\text{O}_3/g\text{-C}_3\text{N}_4$  exhibited similar optical adsorption properties to the pristine  $g\text{-C}_3\text{N}_4$  but the transient photoresponse showed an increased photocurrent for  $\text{In}_2\text{O}_3/g\text{-C}_3\text{N}_4$ . After loading Pt as an electron sink over 10%  $\text{In}_2\text{O}_3/g\text{-C}_3\text{N}_4$ , 159.2 ppm  $\text{CH}_4$  can be evolved for 4 h. Transient PL decay indicated the inhibited charge recombination in  $\text{In}_2\text{O}_3/g\text{-C}_3\text{N}_4$  due to enhanced charge

separation at the interface. In another study, a  $g\text{-C}_3\text{N}_4/\text{TiO}_2$  heterojunction was prepared by an *in situ* growth method.<sup>105</sup> The surface area of the composite increased with the percentage of  $\text{TiO}_2$  in the composite. When the photoreduction of  $\text{CO}_2$  was carried out with water vapor without a cocatalyst under UV-vis irradiation, CO was found to be the main product although a small amount of  $\text{CH}_4$  was also produced.  $\text{Bi}_2\text{WO}_6$  was previously prepared by a hydrothermal method and shown active for the reduction of  $\text{CO}_2$  into CO under visible light.<sup>106</sup> A solvothermal process was used to grow  $\text{Bi}_2\text{WO}_6$  *in situ* to form a  $g\text{-C}_3\text{N}_4/\text{Bi}_2\text{WO}_6$  composite.<sup>107</sup> The measured CB and VB positions of  $g\text{-C}_3\text{N}_4$  and  $\text{Bi}_2\text{WO}_6$  were used to explain the possible mechanism for the photoreduction of  $\text{CO}_2$  to CO. Compared to the pure  $\text{Bi}_2\text{WO}_6$  prepared using the hydrothermal or solvothermal method, the activity of the composite was largely enhanced. ZnO, a large band gap semiconductor, was also used to make a composite with  $g\text{-C}_3\text{N}_4$  by an impregnation method for  $\text{CO}_2$  reduction. The charge separation and transportation were promoted by the suitable band alignment between  $g\text{-C}_3\text{N}_4$  and ZnO, which leads to an enhanced activity.<sup>108</sup> Besides oxides, carbon materials have also been coupled with  $g\text{-C}_3\text{N}_4$  for  $\text{CO}_2$  photoreduction. For example, a sandwich-like graphene/ $g\text{-C}_3\text{N}_4$  hybrid nanostructure was fabricated using graphene oxide as a structure directing agent.<sup>109</sup> The hybrid material shows enhanced activity for the conversion of  $\text{CO}_2$  to  $\text{CH}_4$  in the presence of water vapor under a daylight lamp. The enhanced photoactivity was attributed to the improved electron transfer induced by graphene.

Besides the electronic and catalytic aspects, modifying  $g\text{-C}_3\text{N}_4$  with a component for  $\text{CO}_2$  adsorption and enrichment has been found effective in enhancing the performance of the overall system. For example, Wang *et al.* coupled  $g\text{-C}_3\text{N}_4$  with a Co-containing zeolitic imidazole framework (Co-ZIF).<sup>110</sup> Co-ZIF-9 has a high  $\text{CO}_2$  adsorption capacity of 2.7 mmol  $\text{g}^{-1}$  and affords a high microporous surface area of 1607  $\text{m}^2 \text{g}^{-1}$ . As a result, Co-ZIF-9 can capture and concentrate  $\text{CO}_2$  in its pores. After an electron mediator, bipyridine, was added into the reaction solution; the photoexcited electrons can be transferred from  $g\text{-C}_3\text{N}_4$  to Co-ZIF-9 for  $\text{CO}_2$  reduction as revealed by PL quenching study. CO was the main product in this system and a QE of 0.9% can be obtained, even without the loading of a cocatalyst. Our group reported the construction of a hybrid system using  $g\text{-C}_3\text{N}_4$  and an anionic clay called layered double hydroxide (LDH) which has high affinity for  $\text{CO}_2$ .<sup>111</sup> The structure of the LDH/ $g\text{-C}_3\text{N}_4$  composite is shown in Fig. 10A. Mg-Al-LDH with a positive surface charge was assembled with oppositely charged  $g\text{-C}_3\text{N}_4$  by electrostatic interactions. In the TEM image shown in Fig. 10B, the hexagonal-shaped LDH nanosheets can be seen on the surface of  $g\text{-C}_3\text{N}_4$ . Due to its unique layered structure,  $\text{CO}_2$  molecules can be intercalated in the interlayer space of LDH in the form of  $\text{CO}_3^{2-}$  anions. After loading Pd as the cocatalyst,  $\text{CH}_4$  was the main product for  $\text{CO}_2$  reduction using this photocatalyst under UV-vis light. Isotopic measurement and blank control experiment

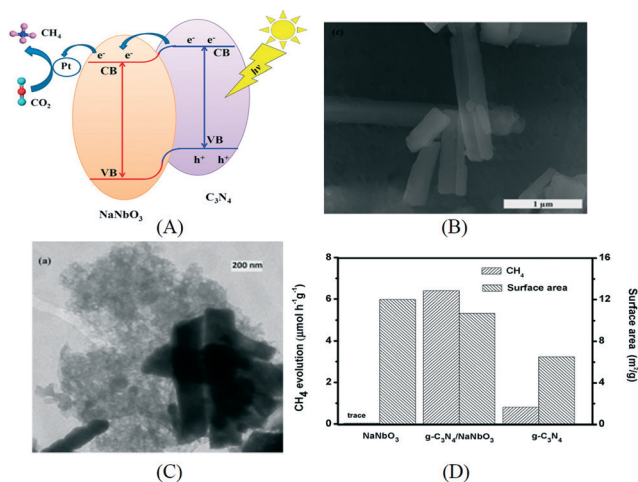
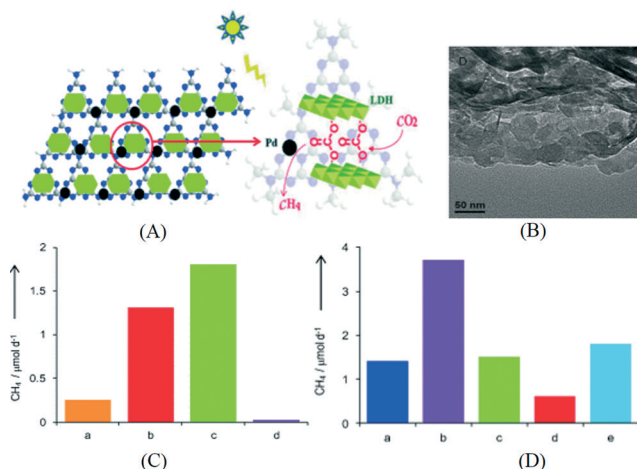


Fig. 9 (A) Schematics of energy diagram of  $\text{NaNbO}_3/g\text{-C}_3\text{N}_4$ ; (B) SEM image and (C) TEM image of  $\text{NaNbO}_3/g\text{-C}_3\text{N}_4$ ; (D) photocatalytic  $\text{CO}_2$  reduction and surface area of  $\text{NaNbO}_3/g\text{-C}_3\text{N}_4$ . Reprinted with permission from ref. 103. Copyright 2015 American Chemical Society.





**Fig. 10** (A) Schematics of the structure of Mg-Al-LDH/g-C<sub>3</sub>N<sub>4</sub>; (B) TEM image of Mg-Al-LDH/g-C<sub>3</sub>N<sub>4</sub>; (C) CO<sub>2</sub> reduction activity of Pd loaded photocatalysts: a. LDH-NO<sub>3</sub><sup>-</sup>/g-C<sub>3</sub>N<sub>4</sub>, b. LDH/g-C<sub>3</sub>N<sub>4</sub>, c. LDH-CO<sub>3</sub><sup>2-</sup>/g-C<sub>3</sub>N<sub>4</sub>, d. g-C<sub>3</sub>N<sub>4</sub>; (D) CO<sub>2</sub> reduction activity of Pd loaded photocatalysts: a. g-C<sub>3</sub>N<sub>4</sub>, b. Mg-Al-LDH/g-C<sub>3</sub>N<sub>4</sub>, c. Zn-Al-LDH/g-C<sub>3</sub>N<sub>4</sub>, d. Ni-Al-LDH/g-C<sub>3</sub>N<sub>4</sub>, e. Zn-Cr-LDH/g-C<sub>3</sub>N<sub>4</sub>.<sup>111</sup> Copyright 2014 WILEY-VCH Verlag GmbH & Co. KGaA Weinheim.

indicated that most of the evolved CH<sub>4</sub> was from CO<sub>2</sub> instead of other carbon-containing species. The photocatalytic activity of the assembly system is 4 times that of the control sample without LDH. Among the LDHs intercalated with dominant NO<sub>3</sub><sup>-</sup>, dominant CO<sub>3</sub><sup>2-</sup> and the mixture of the two, LDH-CO<sub>3</sub><sup>2-</sup> shows superior performance (Fig. 10C), suggesting that the intercalated CO<sub>3</sub><sup>2-</sup> anions from dissolved CO<sub>2</sub> in water can act as a carbon source and are easily reduced since LDH is in close contact with both g-C<sub>3</sub>N<sub>4</sub> and Pd. As shown in Fig. 10D, LDHs with different metal compositions were compared and Mg-Al-LDH exhibited the best performance for CO<sub>2</sub> reduction which correlates with the highest CO<sub>2</sub> adsorption capacity of Mg-Al-LDH among all LDHs. The highest QE of 0.093% was obtained at 440 nm over the optimized Pd/LDH/g-C<sub>3</sub>N<sub>4</sub> assembly. The QE is still low but this example shows that the concept of coupling g-C<sub>3</sub>N<sub>4</sub> with a CO<sub>2</sub> capturing material is promising in CO<sub>2</sub> reduction.

In summary, the study of g-C<sub>3</sub>N<sub>4</sub> based photocatalysts for CO<sub>2</sub> reduction is still at its early stage, but has received increasing interests in recent years. Different g-C<sub>3</sub>N<sub>4</sub> based photocatalysts were synthesized including organic-inorganic hybrids, metal deposited g-C<sub>3</sub>N<sub>4</sub>, nanocomposites of g-C<sub>3</sub>N<sub>4</sub> with oxides or carbon materials, and composites of g-C<sub>3</sub>N<sub>4</sub> with CO<sub>2</sub> adsorbing materials. The photocatalytic activity of g-C<sub>3</sub>N<sub>4</sub> based photocatalysts depends on many factors and continuous efforts are needed for the development of more efficient and stable photocatalysts for CO<sub>2</sub> reduction. It is also worth noting that the reported experimental setups, reaction conditions and product analysis methods vary from one paper to another. This makes it difficult to directly compare the reported activity data from different research groups. While it is challenging to adopt the same experimental setup by different groups, it is important to use reliable

methods to accurately quantify various products of CO<sub>2</sub> reduction. Several review articles including ours published in the past few years on this topic can provide useful practical guidelines to researchers in this field.<sup>112–114</sup>

## 6. Conclusion and outlook

This mini review summarizes the latest research efforts on the development of g-C<sub>3</sub>N<sub>4</sub> based photocatalyst systems with the emphasis on the development of non-noble metal cocatalysts for g-C<sub>3</sub>N<sub>4</sub>, exfoliation of g-C<sub>3</sub>N<sub>4</sub> to nanosheets with enhanced photoactivity, and application of g-C<sub>3</sub>N<sub>4</sub> based photocatalysts for water oxidation, overall water splitting and CO<sub>2</sub> reduction. The study of non-noble metal cocatalyst loaded g-C<sub>3</sub>N<sub>4</sub> has already achieved some breakthroughs. The activities of a few photocatalysts like MoS<sub>2</sub>/g-C<sub>3</sub>N<sub>4</sub> and Ni(OH)<sub>2</sub>/g-C<sub>3</sub>N<sub>4</sub> were reported to approach or surpass that of Pt/g-C<sub>3</sub>N<sub>4</sub>. Further improvement of efficiency and stability is still in need. Exfoliation is a promising method to improve the photocatalytic activity of g-C<sub>3</sub>N<sub>4</sub>. Facile and simple liquid exfoliation can be conducted in water, certain organic solvents or acid solutions. Single layered or few layered g-C<sub>3</sub>N<sub>4</sub> nanosheets can be obtained after exfoliation. The larger surface area, improved charge transfer ability and enhanced charge separation contribute to the superior photocatalytic activities of g-C<sub>3</sub>N<sub>4</sub> nanosheets. The performance can be further improved by preparing porous g-C<sub>3</sub>N<sub>4</sub> nanosheets. However, the current exfoliation method suffers from long sonication time and low yield. It is necessary to develop more efficient exfoliation methods. Water oxidation can be achieved by g-C<sub>3</sub>N<sub>4</sub> based photocatalysts such as cobalt oxide loaded g-C<sub>3</sub>N<sub>4</sub>, although there are only limited research works on water oxidation over g-C<sub>3</sub>N<sub>4</sub>. The performance and stability of current g-C<sub>3</sub>N<sub>4</sub> water oxidation photocatalysts are quite poor. Meanwhile, the study of overall water splitting by g-C<sub>3</sub>N<sub>4</sub> based photocatalysts is in its early stage although some systems including single particulate systems and Z-schemes have been shown capable of evolving stoichiometric H<sub>2</sub> and O<sub>2</sub> from water. Further development of efficient g-C<sub>3</sub>N<sub>4</sub> based photocatalysts for water oxidation is thus needed for their application in overall water splitting. There have been increasing research interests in CO<sub>2</sub> photoreduction using g-C<sub>3</sub>N<sub>4</sub> due to its suitable electronic band structure. Drawbacks including moderate optical adsorption properties, low charge carrier mobility, inert surface, low surface area and rich grain boundary defects need to be overcome to improve its photocatalytic activity. Some innovative ways and more systematic work are probably required to develop g-C<sub>3</sub>N<sub>4</sub> to efficient and stable photocatalysts, which is a challenging task.

## Acknowledgements

This work was supported by Nanyang Technological University. S. M. Yin acknowledges the research scholarship from Nanyang Technological University.



## Notes and references

- 1 D. Kim, K. K. Sakimoto, D. Hong and P. Yang, *Angew. Chem., Int. Ed.*, 2015, **54**, 3259.
- 2 T. Hisatomi, J. Kubota and K. Domen, *Chem. Soc. Rev.*, 2014, **43**, 7520.
- 3 S. N. Habisreutinger, L. Schmidt-Mende and J. K. Stolarczyk, *Angew. Chem., Int. Ed.*, 2013, **52**, 7372.
- 4 A. Fujishima and K. Honda, *Nature*, 1972, **238**, 37.
- 5 A. Kudo and Y. Miseki, *Chem. Soc. Rev.*, 2009, **38**, 253.
- 6 F. E. Osterloh, *Chem. Soc. Rev.*, 2013, **42**, 2294.
- 7 K. Maeda and K. Domen, *MRS Bull.*, 2011, **36**, 25.
- 8 A. J. Morris, G. J. Meyer and E. Fujita, *Acc. Chem. Res.*, 2009, **42**, 1983.
- 9 S. Cao, J. Low, J. Yu and M. Jaroniec, *Adv. Mater.*, 2015, **27**, 2150.
- 10 Y. Wang, X. C. Wang and M. Antonietti, *Angew. Chem., Int. Ed.*, 2012, **51**, 68.
- 11 X. C. Wang, K. Maeda, A. Thomas, K. Takanabe, G. Xin, J. M. Carlsson, K. Domen and M. Antonietti, *Nat. Mater.*, 2009, **8**, 76.
- 12 Y. Moriya, T. Takata and K. Domen, *Coord. Chem. Rev.*, 2013, **257**, 1957.
- 13 X. Ma, Y. Lv, J. Xu, Y. Liu, R. Zhang and Y. Zhu, *J. Phys. Chem. C*, 2012, **116**, 23485.
- 14 Y. Zhang, T. Mori, J. Ye and M. Antonietti, *J. Am. Chem. Soc.*, 2010, **132**, 6294.
- 15 G. Liu, P. Niu, C. Sun, S. C. Smith, Z. Chen, G. Q. M. Lu and H. Cheng, *J. Am. Chem. Soc.*, 2010, **132**, 11642.
- 16 G. Dong, K. Zhao and L. Zhang, *Chem. Commun.*, 2012, **48**, 6178.
- 17 Y. Zhang, T. Mori and J. Ye, *Sci. Adv. Mater.*, 2012, **4**, 282.
- 18 Z. Lin and X. Wang, *Angew. Chem., Int. Ed.*, 2013, **52**, 1735.
- 19 M. Zhang and X. Wang, *Energy Environ. Sci.*, 2014, **7**, 1902.
- 20 X. Wang, X. Chen, A. Thomas, X. Fu and M. Antonietti, *Adv. Mater.*, 2009, **21**, 1609.
- 21 G. Zhang, M. Zhang, X. Ye, X. Qiu, S. Lin and X. Wang, *Adv. Mater.*, 2014, **26**, 805.
- 22 J. Hong, X. Xia, Y. Wang and R. Xu, *J. Mater. Chem.*, 2012, **22**, 15006.
- 23 P. Martin-Ramos, J. Martin-Gil, R. Dante, F. Vaquero, R. Navarro and J. Fierro, *Int. J. Hydrogen Energy*, 2015, **40**, 7273.
- 24 Y. Zhang, T. Mori, L. Niu and J. Ye, *Energy Environ. Sci.*, 2011, **4**, 4517.
- 25 Q. Xiang, J. Yu and M. Jaroniec, *J. Phys. Chem. C*, 2011, **115**, 7355.
- 26 A. Du, S. Sanvito, Z. Li, D. Wang, Y. Jiao, T. Liao, Q. Sun, Y. H. Ng, Z. Zhu, R. Amal and S. C. Smith, *J. Am. Chem. Soc.*, 2012, **134**, 4393.
- 27 X. Wang, J. Chen, X. Guan and L. Guo, *Int. J. Hydrogen Energy*, 2015, **40**, 7546.
- 28 Z. Zhao, Y. Sun and F. Dong, *Nanoscale*, 2015, **7**, 15.
- 29 Y. Wang, J. Hong, W. Zhang and R. Xu, *Catal. Sci. Technol.*, 2013, **3**, 1703.
- 30 L. Ge, F. Zuo, J. Liu, Q. Ma, C. Wang, D. Sun, L. Bartels and P. Feng, *J. Phys. Chem. C*, 2012, **116**, 13708.
- 31 X. Wang, K. Maeda, X. Chen, K. Takanabe, K. Domen, Y. Hou, X. Fu and M. Antonietti, *J. Am. Chem. Soc.*, 2009, **131**, 1680.
- 32 J. Zhang, M. Zhang, C. Yang and X. Wang, *Adv. Mater.*, 2014, **26**, 4121.
- 33 Y. Cui, Z. Ding, X. Fu and X. Wang, *Angew. Chem., Int. Ed.*, 2012, **51**, 11814.
- 34 X. Li, X. Wang and M. Antonietti, *Chem. Sci.*, 2012, **3**, 2170.
- 35 X. Bai, L. Wang, R. Zong and Y. Zhu, *J. Phys. Chem. C*, 2013, **117**, 9952.
- 36 D. Zheng, C. Pang, Y. Liu and X. Wang, *Chem. Commun.*, 2015, **51**, 9706.
- 37 J. H. Sun, J. S. Zhang, M. W. Zhang, M. Antonietti, X. Z. Fu and X. C. Wang, *Nat. Commun.*, 2012, **3**, 1139.
- 38 J. Zhang, F. Guo and X. Wang, *Adv. Funct. Mater.*, 2013, **23**, 3008.
- 39 S. Cao and J. Yu, *J. Phys. Chem. Lett.*, 2014, 2101.
- 40 J. Yang, D. Wang, H. Han and C. Li, *Acc. Chem. Res.*, 2013, **46**, 1900.
- 41 J. Ran, J. Zhang, J. Yu, M. Jaroniec and S. Z. Qiao, *Chem. Soc. Rev.*, 2014, **43**, 7787.
- 42 J. Dong, M. Wang, X. Li, L. Chen, Y. He and L. Sun, *ChemSusChem*, 2012, **5**, 2133.
- 43 D. Wang, Y. Zhang and W. Chen, *Chem. Commun.*, 2014, **50**, 1754.
- 44 J. Huang, K. L. Mulfort, P. Du and L. X. Chen, *J. Am. Chem. Soc.*, 2012, **134**, 16472.
- 45 S. Cao, X. Liu, Y. Yuan, Z. Zhang, J. Fang, S. C. J. Loo, J. Barber, T. C. Sum and C. Xue, *Phys. Chem. Chem. Phys.*, 2013, **15**, 18363.
- 46 S. Cao, Y. Yuan, J. Barber, S. C. J. Loo and C. Xue, *Appl. Surf. Sci.*, 2014, **319**, 344.
- 47 J. Hong, Y. Wang, Y. Wang, W. Zhang and R. Xu, *ChemSusChem*, 2013, **6**, 2263.
- 48 Z. Chen, P. Sun, B. Fan, Z. Zhang and X. Fang, *J. Phys. Chem. C*, 2014, **118**, 7801.
- 49 L. Yin, Y. Yuan, S. Cao, Z. Zhang and C. Xue, *RSC Adv.*, 2014, **4**, 6127.
- 50 Y. Zhu, Y. Xu, Y. Hou, Z. Ding and X. Wang, *Int. J. Hydrogen Energy*, 2014, **39**, 11873.
- 51 H. Vrubel, D. Merki and X. Hu, *Energy Environ. Sci.*, 2012, **5**, 6136.
- 52 Y. Hou, A. B. Laursen, J. Zhang, G. Zhang, Y. Zhu, X. Wang, S. Dahl and I. Chorkendorff, *Angew. Chem., Int. Ed.*, 2013, **52**, 3621.
- 53 Y. Hou, Y. Zhu, Y. Xu and X. Wang, *Appl. Catal., B*, 2014, **156–157**, 122.
- 54 J. Yu, S. Wang, B. Cheng, Z. Lin and F. Huang, *Catal. Sci. Technol.*, 2013, **3**, 1782.
- 55 X. Zhou, Z. Luo, P. Tao, B. Jin, Z. Wu and Y. Huang, *Mater. Chem. Phys.*, 2014, **143**, 1462.
- 56 G. Zhang, G. Li and X. Wang, *ChemCatChem*, 2015, DOI: 10.1002/cctc.201500069.



- 57 P. Niu, L. Zhang, G. Liu and H. Cheng, *Adv. Funct. Mater.*, 2012, 22, 4763.
- 58 H. Xu, J. Yan, X. She, L. Xu, J. Xia, Y. Xu, Y. Song, L. Huang and H. Li, *Nanoscale*, 2014, 6, 1406.
- 59 X. Zhang, X. Xie, H. Wang, J. Zhang, B. Pan and Y. Xie, *J. Am. Chem. Soc.*, 2012, 135, 18.
- 60 J. Tian, Q. Liu, A. M. Asiri, A. O. Al-Youbi and X. Sun, *Anal. Chem.*, 2013, 85, 5595.
- 61 N. Cheng, J. Tian, Q. Liu, C. Ge, A. H. Qusti, A. M. Asiri, A. O. Al-Youbi and X. Sun, *ACS Appl. Mater. Interfaces*, 2013, 5, 6815.
- 62 H. Zhang, L. Guo, L. Zhao, B. Wan and Y. Yang, *J. Phys. Chem. Lett.*, 2015, 958.
- 63 S. Yang, Y. Gong, J. Zhang, L. Zhan, L. Ma, Z. Fang, R. Vajtai, X. Wang and P. M. Ajayan, *Adv. Mater.*, 2013, 25, 2452.
- 64 X. She, H. Xu, Y. Xu, J. Yan, J. Xia, L. Xu, Y. Song, Y. Jiang, Q. Zhang and H. Li, *J. Mater. Chem. A*, 2014, 2, 2563.
- 65 Q. Lin, L. Li, S. Liang, M. Liu, J. Bi and L. Wu, *Appl. Catal., B*, 2015, 163, 135.
- 66 H. Zhao, H. Yu, X. Quan, S. Chen, Y. Zhang, H. Zhao and H. Wang, *Appl. Catal., B*, 2014, 152–153, 46.
- 67 J. Hong, S. Yin, Y. Pan, J. Han, T. Zhou and R. Xu, *Nanoscale*, 2014, 6, 14984.
- 68 K. Chang, M. Li, T. Wang, S. Ouyang, P. Li, L. Liu and J. Ye, *Adv. Energy Mater.*, 2015, 5, 1402279.
- 69 J. Xu, L. Zhang, R. Shi and Y. Zhu, *J. Mater. Chem. A*, 2013, 1, 14766.
- 70 F. Cheng, H. Wang and X. Dong, *Chem. Commun.*, 2015, 51, 7176.
- 71 J. Duan, S. Chen, M. Jaroniec and S. Z. Qiao, *ACS Nano*, 2015, 9, 931.
- 72 Y. Hou, F. Zuo, A. P. Dagg, J. Liu and P. Feng, *Adv. Mater.*, 2014, 26, 5043.
- 73 Y. Zhao, F. Zhao, X. Wang, C. Xu, Z. Zhang, G. Shi and L. Qu, *Angew. Chem., Int. Ed.*, 2014, 53, 13934.
- 74 T. Y. Ma, S. Dai, M. Jaroniec and S. Z. Qiao, *Angew. Chem., Int. Ed.*, 2014, 53, 7281.
- 75 F. Zhang, A. Yamakata, K. Maeda, Y. Moriya, T. Takata, J. Kubota, K. Teshima, S. Oishi and K. Domen, *J. Am. Chem. Soc.*, 2012, 134, 8348.
- 76 K. Maeda, X. Wang, Y. Nishihara, D. Lu, M. Antonietti and K. Domen, *J. Phys. Chem. C*, 2009, 113, 4940.
- 77 A. B. Jorge, D. J. Martin, M. T. S. Dhanoa, A. S. Rahman, N. Makwana, J. Tang, A. Sella, F. Corà, S. Firth, J. A. Darr and P. F. McMillan, *J. Phys. Chem. C*, 2013, 117, 7178.
- 78 M. Walter, E. Warren, J. McKone, S. Boettcher, Q. Mi, E. Santori and N. Lewis, *Chem. Rev.*, 2010, 110, 6446.
- 79 J. Zhang, J. Sun, K. Maeda, K. Domen, P. Liu, M. Antonietti, X. Fu and X. Wang, *Energy Environ. Sci.*, 2011, 4, 675.
- 80 J. Zhang, M. Grzelczak, Y. Hou, K. Maeda, K. Domen, X. Fu, M. Antonietti and X. Wang, *Chem. Sci.*, 2012, 3, 443.
- 81 G. Zhang, S. Zang and X. Wang, *ACS Catal.*, 2015, 941.
- 82 R. Lee, P. D. Tran, S. S. Pramana, S. Y. Chiam, Y. Ren, S. Meng, L. H. Wong and J. Barber, *Catal. Sci. Technol.*, 2013, 3, 1694.
- 83 A. Kudo, *MRS Bull.*, 2011, 36, 32.
- 84 D. J. Martin, P. J. T. Reardon, S. J. A. Moniz and J. Tang, *J. Am. Chem. Soc.*, 2014, 136, 12568.
- 85 G. Zhang, X. Huang, F. Fina, G. Zhang and J. Irvine, *Catal. Sci. Technol.*, 2015, 5, 3416.
- 86 J. Liu, Y. Liu, N. Liu, Y. Han, X. Zhang, H. Huang, Y. Lifshitz, S. Lee, J. Zhong and Z. Kang, *Science*, 2015, 347, 970.
- 87 L. Liao, Q. Zhang, Z. Su, Z. Zhao, Y. Wang, Y. Li, X. Lu, D. Wei, G. Feng, Q. Yu, X. Cai, J. Zhao, Z. Ren, H. Fang, F. Robles-Hernandez, S. Baldelli and J. Bao, *Nat. Nanotechnol.*, 2013, 9, 69.
- 88 Q. Xiang, B. Cheng and J. Yu, *Angew. Chem., Int. Ed.*, 2015, DOI: 10.1002/anie.201411069.
- 89 K. Li, X. An, L. Park, M. Khraisheh and J. Tang, *Catal. Today*, 2014, 224, 3.
- 90 L. Yuan and Y. Xu, *Appl. Surf. Sci.*, 2015, 342, 154.
- 91 X. Li, J. Wen, J. Low, Y. Fang and J. Yu, *Sci. China Mater.*, 2014, 57, 70.
- 92 G. Dong and L. Zhang, *J. Mater. Chem.*, 2012, 22, 1160.
- 93 J. Mao, T. Peng, X. Zhang, K. Li, L. Ye and L. Zan, *Catal. Sci. Technol.*, 2013, 3, 1253.
- 94 K. Wang, Q. Li, B. Liu, B. Cheng, W. Ho and J. Yu, *Appl. Catal., B*, 2015, 176–177, 44.
- 95 K. Maeda, K. Sekizawa and O. Ishitani, *Chem. Commun.*, 2013, 49, 10127.
- 96 K. Sekizawa, K. Maeda, K. Domen, K. Koike and O. Ishitani, *J. Am. Chem. Soc.*, 2013, 135, 4596.
- 97 Y. Tamaki, T. Morimoto, K. Koike and O. Ishitani, *Proc. Natl. Acad. Sci. U. S. A.*, 2012, 109, 15673.
- 98 R. Kuriki, K. Sekizawa, O. Ishitani and K. Maeda, *Angew. Chem., Int. Ed.*, 2015, 54, 2406.
- 99 K. Maeda, R. Kuriki, M. Zhang, X. Wang and O. Ishitani, *J. Mater. Chem. A*, 2014, 2, 15146.
- 100 J. Lin, Z. Pan and X. Wang, *ACS Sustainable Chem. Eng.*, 2014, 2, 353.
- 101 J. Yu, K. Wang, W. Xiao and B. Cheng, *Phys. Chem. Chem. Phys.*, 2014, 16, 11492.
- 102 W. Ong, L. Tan, S. Chai and S. Yong, *Dalton Trans.*, 2015, 44, 1249.
- 103 H. Shi, G. Chen, C. Zhang and Z. Zou, *ACS Catal.*, 2014, 4, 3637.
- 104 S. Cao, X. Liu, Y. Yuan, Z. Zhang, Y. Liao, J. Fang, S. C. J. Loo, T. C. Sum and C. Xue, *Appl. Catal., B*, 2014, 147, 940.
- 105 S. Zhou, Y. Liu, J. Li, Y. Wang, G. Jiang, Z. Zhao, D. Wang, A. Duan, J. Liu and Y. Wei, *Appl. Catal., B*, 2014, 158–159, 20.
- 106 Z. Sun, Z. Yang, H. Liu, H. Wang and Z. Wu, *Appl. Surf. Sci.*, 2014, 315, 360.
- 107 M. Li, L. Zhang, X. Fan, Y. Zhou, M. Wu and J. Shi, *J. Mater. Chem. A*, 2015, 3, 5189.
- 108 Y. He, Y. Wang, L. Zhang, B. Teng and M. Fan, *Appl. Catal., B*, 2015, 168–169, 1.
- 109 W. Ong, L. Tan, S. Chai and S. Yong, *Chem. Commun.*, 2015, 51, 858.



- 110 S. Wang, J. Lin and X. Wang, *Phys. Chem. Chem. Phys.*, 2014, **16**, 14656.
- 111 J. Hong, W. Zhang, Y. Wang, T. Zhou and R. Xu, *ChemCatChem*, 2014, **6**, 2315.
- 112 J. Hong, W. Zhang, J. Ren and R. Xu, *Anal. Methods*, 2012, 1086.
- 113 A. Corma and H. Garcia, *J. Catal.*, 2013, **308**, 168.
- 114 J. A. Herron, J. Kim, A. A. Upadhye, G. W. Huber and C. T. Maravelias, *Energy Environ. Sci.*, 2015, **8**, 126.

